Emission Spectroscopy of Plasma During Laser Welding of AISI 201 Stainless Steel

M.M. COLLUR and T. DEBROY

The rates of vaporization of alloying elements from the weld pool were related to the emission spectra of the plasma during pulsed laser welding of AISI 201 stainless steel under various welding conditions. The temperature distribution in the plasma was determined from the spectra obtained from various locations in the plasma plume. The extent of ionization of the plasma was calculated from the electron temperatures. To understand the role of surface active elements, emission spectra and the vaporization rate of iron that resulted from the welding of ultrapure iron samples were compared with those from the welding of oxidized samples or samples that were doped with sulfur or oxygen.

I. INTRODUCTION

THE loss of volatile alloying elements from the weld pool is a serious problem in the laser welding of many important engineering alloys. If an alloy contains one or more volatile components, its fabrication using a high power density laser beam leads to significant vaporization of alloying elements and inadequate control of composition and properties of the weld. Pronounced changes in the alloy composition due to laser welding of important aluminum alloys[1] and high manganese stainless steels[2] are familiar examples of this problem.

In a recent publication,[3] we discussed the mechanism of alloying element vaporization during laser welding of high manganese stainless steels. The vaporization involves transport of alloying elements from the interior of the weld pool to the surface, aided by the recirculating fluid motion in the weld pool. It was demonstrated that for a given temperature distribution at the weld pool surface, the rate of vaporization was significantly influenced by the presence of plasma. Indeed, plasma is known to influence the chemical nature of the molten metal surfaces as evidenced by the recent measurements[4] of interfacial tensions between low pressure argon plasma and molten iron and copper.

The importance of the role of plasma in welding is well documented in the literature. Weld properties are known to be influenced by the characteristics of the plasma formed during welding.[5] Most of the previous work on the characterization of plasma was undertaken to identify the species present in the welding arcs and to determine the arc temperature using emission spectroscopy. During arc welding of various iron-based alloys, spectral lines of iron, manganese, chromium, and nickel were identified.[6–12] Mills[13,14] demonstrated that the temperature of the welding arc was in the range of 5000 to 6000 K during GTA welding of 21Cr-6Ni-9Mn (weld current: 100 amperes; electrode gap: 0.06 inch) and 304L stainless steels. Glickstein[7] estimated the arc temperature to be 11,000 K near the cathode and 8000 K toward the anode for a 100 amperes GTA welding arc with a 2 mm arc gap during welding of Ni-Cr-Fe alloy (alloy 600). As a result of the previous work[6–14] on arc welding of iron-based alloys, the species present in the welding arcs and the arc temperature range are now fairly well understood. However, such information has been rather scarce for laser processing. For the pulsed spot laser welding of AISI 1018 steel, Chennat and Albright[15] detected the presence of excited and singly ionized iron atoms in the plasma but did not find any evidence of excitation or ionization of helium or argon. From the analysis of emission spectroscopic data, Rockstroh and Mazumder[16] calculated electron temperatures in excess of 17,000 K in pure argon plasma and in the plasma produced by laser irradiation of aluminum targets in an argon atmosphere at 7 kW. In the power density range from near plasma threshold to 5×10^7 watts/cm^2, Knudston *et al.*[17] determined the electron temperature to be about 8000 K for laser-produced aluminum plasmas. Although emission spectroscopy is a potentially attractive technique for the monitoring of alloying element loss, the alloying element vaporization rates have not been correlated with the emission spectroscopic data in the previous works. Furthermore, the temperature and the extent of ionization of the plasma during pulsed laser welding of iron-based alloys are not available in the literature. Such information is vital for understanding certain crucial features of laser beam-solid interaction such as the attenuation of the laser energy due to the plasma[36] and the extent of vaporization of alloying elements from the weld pool.

The presence of surface active elements such as sulfur and oxygen significantly influences the concentration of free electrons on metallic surfaces and affects the absorption of the carbon dioxide laser beam. The resulting improvement in the heat absorption from the beam to the surface, coupled with the possible chemical changes in the surface layer due to the presence of surface active elements, may significantly affect the rates of vaporization of alloying elements. Although the role of surface active elements on the weld pool geometry is well

M.M. COLLUR, formerly Graduate Student, Pennsylvania State University, is with Allegheny Ludlum Steel Corporation, Brackenridge, PA. T. DEBROY, Associate Professor, is with the Department of Materials Science and Engineering, The Pennsylvania State University, University Park, PA 16802.

This paper is based on a presentation made in the T.B. King Memorial Symposium on "Physical Chemistry in Metals Processing" presented at the Annual Meeting of The Metallurgical Society, Denver, CO, February, 1987, under the auspices of the Physical Chemistry Committee and the PTD/ISS.

documented, the potential role of these elements on the vaporization behavior is not clearly understood.

Emission spectroscopy was used to characterize the plasma during pulsed laser welding of high manganese AISI 201 stainless steel and other iron-based alloys. Experiments were designed to correlate the vaporization rate with the intensities of the peaks corresponding to the different vaporizing species under various welding conditions. To understand the role of surface active elements, emission spectra and the vaporization rate of iron that resulted from the laser welding of ultrapure iron samples were compared with those from the laser irradiation of oxidized samples or from samples that were doped with sulfur or oxygen. The temperature distribution in the plasma was calculated from the spectra obtained from various locations in the plasma. The extent of ionization of the plasma was calculated theoretically from electron temperature.

II. EXPERIMENTAL

Figure 1 is a schematic diagram of the experimental setup used for this study. As can be seen from the figure, the radiation emitted from the plasma is focused on the slit of a monochromator through a convex lens. A kinematically mounted diffraction grating is used to obtain a high resolution spectra. An intensified silicon intensified target (ISIT) detector was used to detect the emission from the plasma through a monochromator. The detector, in turn, was connected through a controller to the optical multichannel analyzer (OMA). A 2.5 mm high band at the center of the 12.5 mm × 12.5 mm square ISIT detector was monitored in order to avoid peripheral effects due to aberrations to prevent increased linewidth and reduced resolution.[18] However, the full width of the ISIT detector was monitored allowing about 300 to 600 Å wavelength range of the spectrum to be recorded at one time. Information from the detector was transferred to the OMA as plots of intensity *vs* wavelength.

The monochromator was first calibrated using an argon lamp (ORIEL Model 6030) and atomic absorption hollow cathode tubes as calibration standards such that each channel of the OMA corresponded to a particular wavelength. Intensities of the peaks were calculated by subtracting the background noise from the observed intensities automatically.

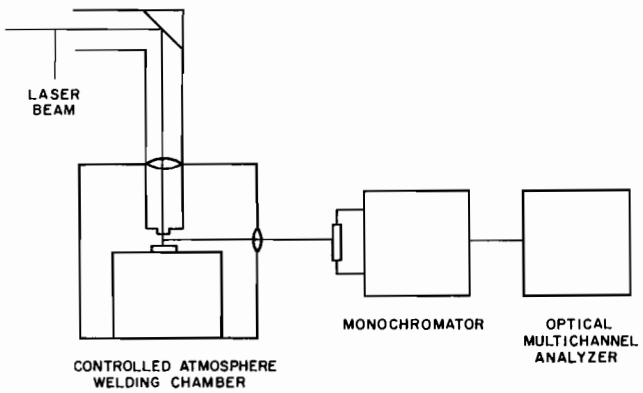

Fig. 1—Schematic diagram of the experimental setup used for this study.

A carbon dioxide laser, Coherent Model Everlase 525-1, was used in the pulsed mode. The samples were placed on a computer-controlled table capable of providing *X-Y* motion. All welding was carried out inside a plexiglass box using a 0.0254 m diameter and 0.127 m focal length Zn-Se lens with an antireflection coating. Most experiments were conducted with a high manganese austenitic stainless steel (AISI 201). The chemical composition of this steel is presented in Table I. Samples of dimensions 0.04 m length, 0.015 m width, and 0.0025 m thickness were welded at a peak power density of about 1.2×10^6 watts/cm^2. Helium was used as the shielding gas. The apparent (time average) vaporization rates were measured by dividing the difference in the weight loss of the sample before and after laser irradiation of the sample with the total laser-solid interaction time. The width and the depth of the weld pool were determined by optical microscopy of the specimen after welding. Since all commercial alloys contain several chemical species in low concentrations, the effects of sulfur and oxygen were studied in ultrapure iron (less than 10 ppm total impurities). Samples were doped with sulfur and oxygen in a high temperature furnace using H_2/H_2S and CO/CO_2 mixtures, respectively. The temperatures and gas compositions utilized for doping were determined on the basis of available thermodynamic data,[19,20] and the values of these parameters are presented in Table II. The oxidized iron samples were prepared by heating specimens in a muffle furnace at 873 K for about two hours. The effect of surface active elements such as sulfur and oxygen on the intensities of the iron peaks was studied using a 600 lines/mm diffraction grating in the monochromator to cover a wide wavelength range of about 600 Å. This was necessary to obtain a large number of peaks at various wavelengths with large differences in the upper energy levels to ensure accuracy in the determination of the plasma temperatures. In the experiments with AISI 201 stainless steel samples, there are many adjacent peaks corresponding to iron, manganese, and chromium. Therefore, a 1200 lines/mm grating covering a wavelength range of about 300 Å was used to achieve good spectral resolution. In order to obtain the radial distribution of temperature, the detector was divided into twenty tracks, and the intensities of two manganese peaks were collected from various radial locations in a thin horizontal slice at the midheight of the plasma, as shown in Figure 2.

Table I. Chemical Composition of AISI 201 Stainless Steel

Element	Wt Pct
Cr	16.34
Ni	4.87
C	0.073
Mn	7.15
Si	0.56
P	0.035
S	0.004
N	0.069
O	0.004
Al	0.003
Fe	Balance

Table II. Experimental Conditions Used for Doping Sulfur and Oxygen in Ultrapure Iron Samples (Time of Experiment = Three Hours)

	Temperature (K)	H_2S/H_2 (Molar Ratio)	CO_2/CO (Molar Ratio)	Wt Pct i
Sulfur doping	1273	5.45×10^{-3}	—	0.013
Oxygen doping	1603	—	0.171	0.002

III. RESULTS AND DISCUSSION

A. *Typical Spectrum*

Figure 3 is a typical spectrum obtained from the plasma produced during laser welding of AISI 201 stainless steel. The intensity of each of the peaks,[21] I_{qp}, is related to the number density of the species (ions or excited neutral atoms), n_{aq}, the probability of transition from the upper energy level q to a lower energy level p, A_{qp}, the frequency of the emission, ν, and the depth of the source, d, and is given by

$$I_{qp} = dA_{qp}n_{aq}h\nu/(4\pi) \quad [1]$$

The number density of the species in the upper energy level q, n_{aq}, is related to the number density of the species in the ground state by the Boltzmann equation:

$$n_{aq} = n_o g_q(e^{(-E_q/kT)})/g_o \quad [2]$$

where n_o is the number density of the species at the ground state, g_q is the degeneracy of the upper energy level, g_o is the degeneracy of the ground state, E_q is the upper energy level, k is the Boltzmann constant, and T is the absolute temperature. It follows from Eqs. [1] and [2] that the intensity of emission at a particular frequency is dependent upon the number density of a species at the ground state, the depth of the plasma domain, and the absolute temperature, the other terms in Eqs. [1] and [2] being constant for a given frequency of emission. Therefore, the intensity of emission is related to the concentration of the species at the ground state, which in turn is influenced by the vaporization rate of the species. Furthermore, the wavelength of emission for a given species is a character of both the upper and the lower energy levels and indicates the state in which the species are present (excited neutral or ionized). From the spectrum in Figure 3, iron, manganese, and chromium were identified in the plasma primarily in their excited neutral states by comparing the wavelengths of various emissions with those given in standard tables.[22] However, a peak corresponding to a singly ionized iron ion is observed at a wavelength of 4233.17 Å. In the wavelength range of the spectrum, this is the only known peak[22] corresponding to the ionized state of iron. The first ionization potentials for manganese and chromium are slightly lower than that for iron. However, in the wavelength range studied, no peak corresponding to ionized state of manganese exists. Although there is a peak corresponding to ionized chromium at a wavelength of 4012.47 Å, its intensity is rather "low," and the peak does not appear in the spectrum. Ionization of iron is documented in the literature[15] during spot welding of AISI 1018 steel in pulsed mode in the power density range similar to the present study. Furthermore, no peak corresponding to helium was detected. It should be noted that helium has a higher first ionization potential (24.5 ev) as compared to iron (7.9 ev), Cr (6.8 ev), or Mn (7.4 ev). The dominance of iron and manganese in the plasma is consistent with the composition of the vaporized species determined by the vapor deposition technique in an independent study[2] performed on a steel of similar composition. The relative quantities of various elements obtained from the analysis are presented in Table III. It is observed that iron and manganese were the most dominant metal vapors, followed by chromium. Nickel was present at a very low concentration.

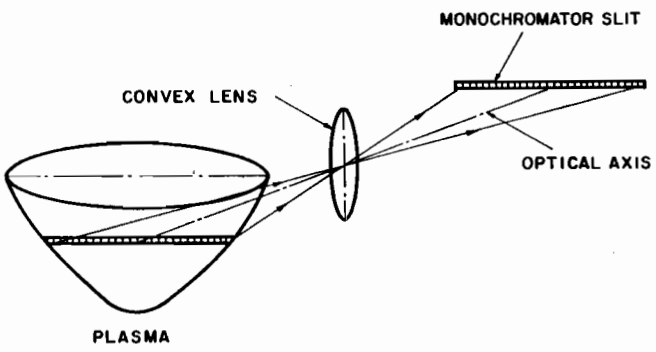

Fig. 2—The experimental arrangement used for the determination of plasma temperature distribution.

B. *Heat Input*

It was pointed out in the earlier section that the intensity of a peak at a particular wavelength is related to the

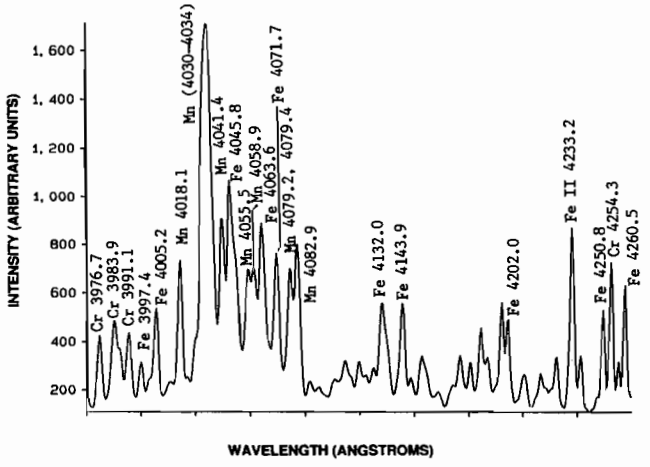

Fig. 3—A typical spectrum of the plasma produced during laser welding of AISI 201 stainless steel using helium gas for shielding the atmosphere. (Gas flow rate = 3.33×10^{-5} m^3/s; welding speed = 0.005 m/s; current = 35 mA; pulse length = 0.003 s; frequency = 100 Hz.)

Table III. Analysis of Vapor Condensate

Laser Power: 560 watts
Welding Speed: 3.5×10^{-3} m/s
Helium Flowrate: 1.0×10^{-4} m^3/s
Composition Ratio (Moles of i/Moles of j)
$J_{Fe}/J_{Mn} = 1.09$
$J_{Cr}/J_{Mn} = 0.58$
$J_{Ni}/J_{Mn} = 0.04$

Note: The above information is obtained from Reference 2.

number density of atoms in the ground state, which in turn is influenced by the rate of vaporization of an alloying element during welding. The relation between the intensity of a peak and the rate of vaporization is demonstrated from the results of the experiments presented in Figures 4(a) and (b). It is observed that the increase in the vaporization rate with the laser energy is accompanied by a concomitant increase in the intensities of several major peaks of iron, manganese, and chromium. However, the correlation between the vaporization rate and the intensities of the peaks is valid only for a constant welding speed, shielding gas flow rate, and composition, as these parameters affect the amount of plasma present above the weld pool. Under the experimental conditions of the present study, the aspect ratio of the weld pool is closely related to the laser energy (Figure 4(c)) and to the intensity of the peaks (Figure 4(a)). These results indicate that under the conditions of the present study, one can monitor the variation in the vaporization rates and the weld pool size from the changes in the intensities of the peaks in the spectrum.

Figure 5(a) depicts the variation of the intensities of Mn, Fe, and Cr peaks with the welding speed. The intensities of the peaks decrease at higher welding speeds due to a decreased heat input and a shorter beam interaction time, resulting in a decrease in the amount of plasma formed. The slight decrease in the weld pool size at higher welding speeds, as shown in Figure 5(b), is also due to a decrease in the beam interaction time. This indicates that the variation in the weld pool size can be detected from the changes in the intensities of the peaks as the two variables, *viz.*, intensity and the weld pool size, exhibit similar responses to the changes in the welding speed under constant laser power, shielding gas flow rate, and composition.

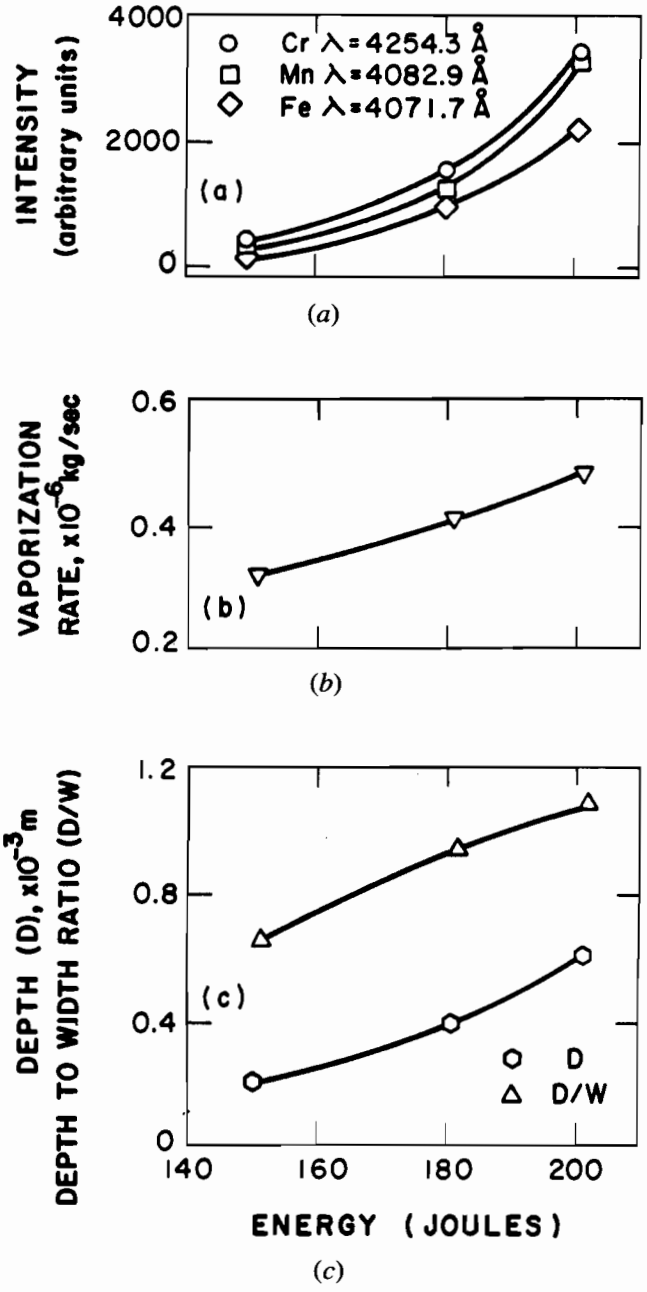

Fig. 4—(*a*) Intensities of the major peaks of Cr, Mn, and Fe as a function of the input laser energy in joules. (*b*) Variation of the vaporization rate with the input laser energy. (*c*) Variation of the depth and the depth/width ratio with the input laser energy. (Gas flow rate = 1.33×10^{-4} m^3/s; welding speed = 0.005 m/s; pulse length = 0.003 s; frequency = 100 Hz.)

C. *Plasma Temperatures*

The determination of electron temperature distribution involves identification of two suitable wavelengths of a single thermometric element in the plasma. The peaks must satisfy the requirement[21] of close proximity of the wavelengths and have a significant difference in the upper energy levels, at least of the order of k*T*. Two manganese peaks corresponding to wavelengths 5377.63 and 5341.06 Å satisfy these requirements and were used by Mills[13,14] for the determination of arc temperatures during GTA welding of high manganese stainless steels. The intensities of these two peaks were determined experimentally at different lateral regions of the plasma at a midheight horizontal plane by placing the monochromator slit horizontally. The experimentally observed intensities along the line of sight of the monochromator slit were then obtained and reduced to ten data points by taking the average of two intensities symmetric to the center. These values are plotted in Figure 6 for both the manganese peaks. Local values of intensities were determined from the observed line-of-sight intensities by a deconvolution scheme using the well-established Abel transformation.[24] The transformation was carried out by a numerical scheme based on Barr's technique[24] with

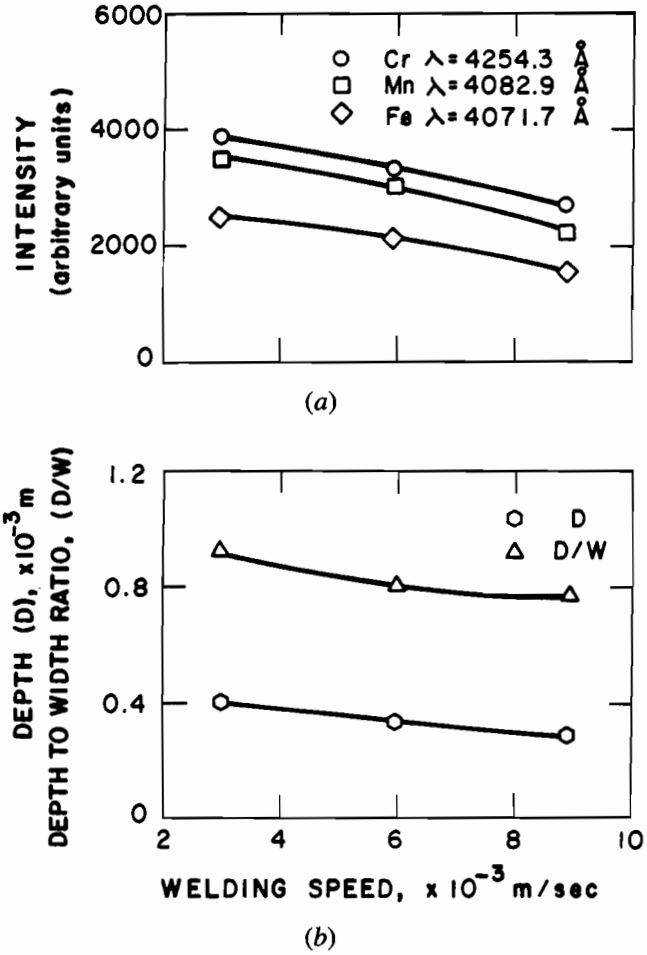

Fig. 5—(*a*) Intensities of the major peaks of Cr, Mn, and Fe as a function of the welding speed. (*b*) Variation of the depth and the depth/width ratio as a function of the welding speed. (Gas flow rate = 3.33×10^{-5} m^3/s; current = 35 mA; pulse length = 0.003 s; frequency = 100 Hz.)

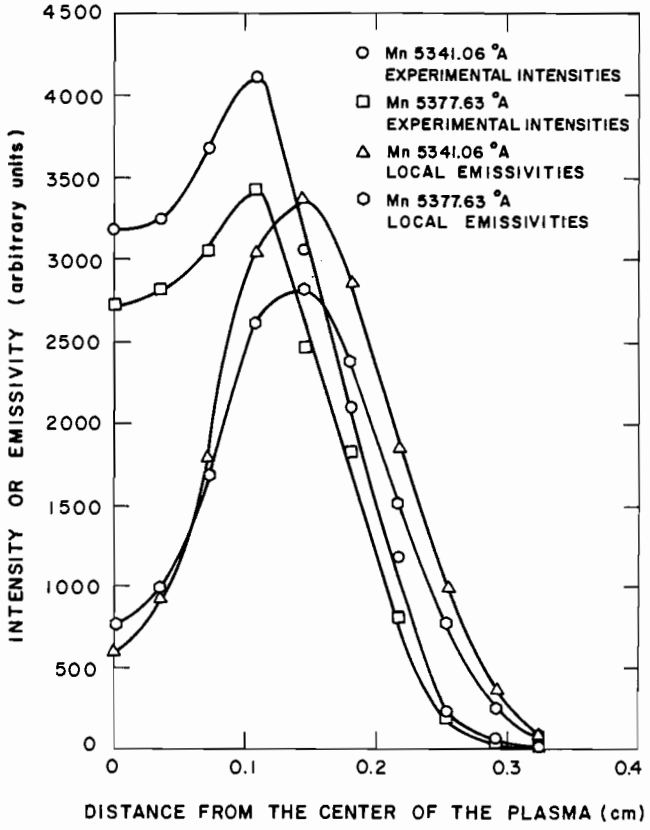

Fig. 6—Plot of the experimental intensities and the local emissivities at various radial locations for the two manganese peaks at 5377.63 and 5341.06 Å. (Gas flow rate = 3.33×10^{-5} m^3/s; welding speed = 0.005 m/s; current = 30 mA; pulse length = 0.003 s; frequency = 100 Hz.)

the help of a computer program developed at Penn State. The computed local emissivities are depicted in Figure 6 for both the manganese peaks. The trend of these plots for the experimentally observed intensities and the inverted local emissivities is similar to that observed by Olsen[35] in studies on argon plasma. The values of local emissivities of the two manganese peaks at each radial location were used for the determination of the radial distribution of the plasma temperature. The plasma was assumed to be optically thin. It will be demonstrated subsequently in this paper that this assumption is reasonable in view of the weak nature of the plasma. The following equation was used for the calculation of radial distribution of electron temperature assuming local thermodynamic equilibrium:

$$T = \frac{5040(V_a - V_b)}{\log\left[\frac{(gA)_a}{(gA)_b}\right] - \log\left(\frac{\lambda_a}{\lambda_b}\right) - \log\left(\frac{J_a}{J_b}\right)} \quad [3]$$

where V is the excitation potential in ev, A is the transition probability, g is the statistical weight, λ is the wavelength, J is the local emissivity, and the subscripts a and b refer to Mn peaks at 5377.63 and 5341.06 Å wavelengths, respectively. The data used for the calculations[25] are presented in Table IV. Figure 7 depicts the computed radial temperature distribution. The distance between the lens and the monochromator slit was adjusted to accommodate the entire image of the plasma on the slit, and the two regions near the boundaries of the plasma were matched with the first and the last track of the sensitized region of the detector. The width of the plasma domain was then determined from the dimension of the sensitized region of the detector and the

Table IV. Data Used for the Calculation of the Plasma Temperature Distribution Using Equation [3]

Wavelength of the peak (Å)	Transition probability ($\times 10^8$ s^{-1})	Statistical Weight	Upper Excitation Potential (ev)	Subscript
5377.63	0.42	4	6.148	a
5341.06	0.014	8	4.435	b

Note: The above information is obtained from Reference 25.

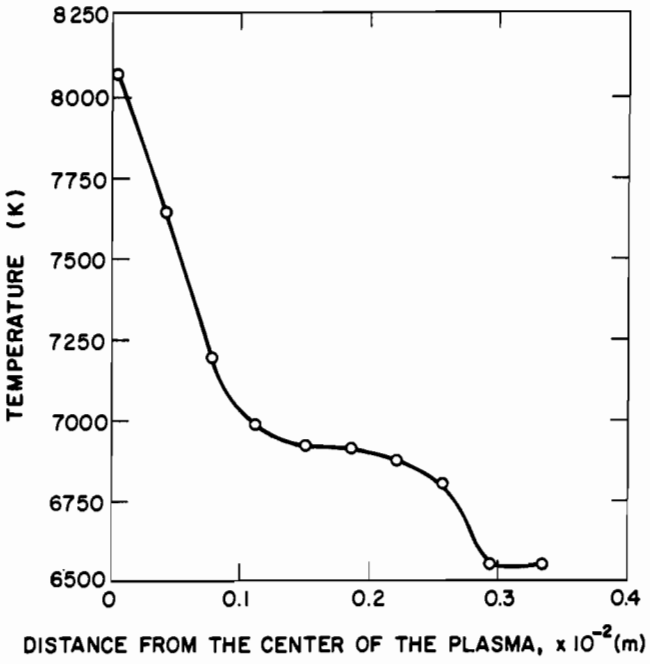

Fig. 7—Plasma temperature distribution as a function of radial distance obtained from the local emissivities after Abel inversion.

magnification due to the convex lens and was found to be about 0.65 cms. It is clear that the plasma temperature varies from about 8100 K at the center to about 6500 K at the periphery. The possible errors in the temperature values are fairly large and are discussed in the Appendix. The temperatures obtained from this analysis are within the range of plasma temperatures calculated theoretically by Pirri *et al.*,[26] who found that the laser plasmas typically reach temperatures of 5000 to 20,000 K. Rockstroh[27] determined peak temperatures of about 17,000 K and about 10,000 K near the end of their plasma core for their laser-produced aluminum-argon plasmas. Under these conditions, the plasma extended approximately 18 mm above the target surface. The relatively high electron temperatures and the large plasma domain are consistent with the use of high laser power in the kilowatt range used in their study.

Figure 8 depicts the spectrum obtained from the plasma produced during laser welding of ultrapure iron samples. This spectrum was collected by placing the monochromator slit vertically, *i.e.*, parallel to the laser beam impingement axis. The determination of plasma temperature distribution from spectroscopic data requires a knowledge of local intensities (emissivities). Since the intensities measured by emission spectroscopy along the line of sight of the spectroscope represent contributions from various locations, a deconvolution scheme is necessary to obtain local intensity values. Appropriate deconvolution schemes such as the Abel transform can be readily applied to determine local emissivities for simple well-defined geometries such as horizontal circular sections of the plasma plume. However, for the vertical planes containing the laser beam impingement axis where the geometry is more complex, deconvolution of line of sight intensities to obtain local intensity values is not a straightforward task. One recourse was to obtain an average plasma temperature along the vertical plane containing the laser beam impingement axis by a technique well documented in most books on plasma diagnostics[21] and used recently by Knudtson *et al.*[17] for laser-produced aluminum plasmas. The following equation[28,29] was used to determine an average plasma temperature:

$$\ln (\varepsilon_{qp}/(g_q A_{qp} \nu)) = \ln (N/Z) - E_q/kT \qquad [4]$$

where ν is the frequency, E_q and g_q are the energy and the degeneracy of the upper energy level, respectively, A_{qp} is the transition probability, k is the Boltzmann constant, T is the absolute temperature, and ε_{qp} is the intensity (area under each peak). The values of g_q, A_{qp}, and E_q at various wavelengths of iron peaks were taken from the work of Fuhr *et al.*[30] The slope of the plot on the left-hand side of Eq. [4] *vs* the upper energy level E_q is a measure of the electron temperature. Figure 9 represents such a plot for the spectrum obtained from the pure iron sample (Figure 8). The slope of the line was

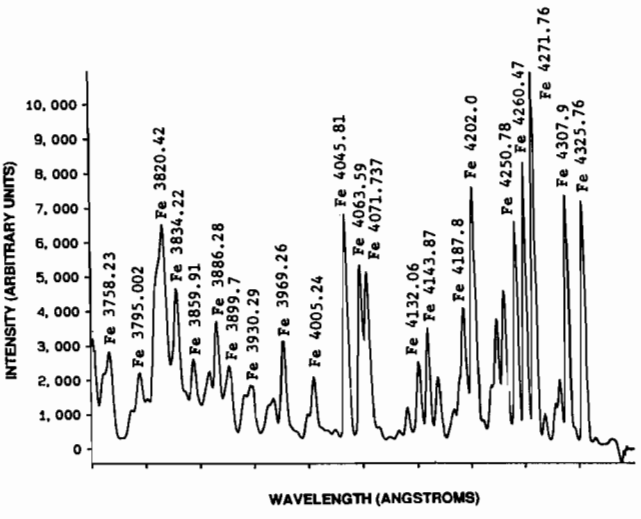

Fig. 8—A typical spectrum of the plasma produced during laser welding of an ultrapure iron sample using helium as the shielding atmosphere. (Gas flow rate = 3.33×10^{-5} m^3/s; welding speed = 0.005 m/s; current = 35 mA; pulse length = 0.003 s; frequency = 100 Hz.)

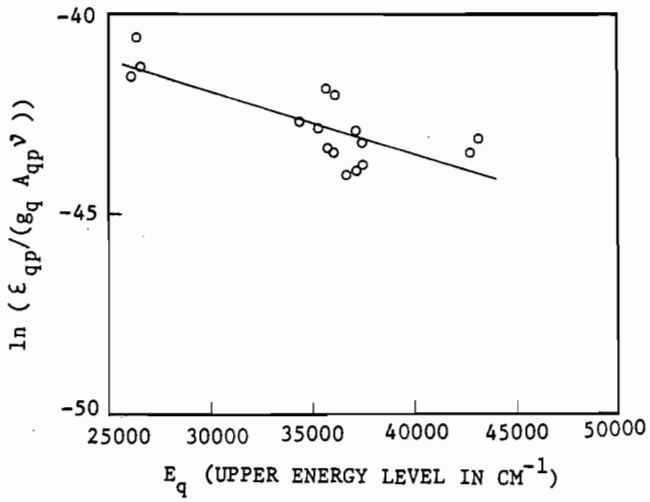

Fig. 9—Plot of the left-hand side of Eq. [4] *vs* the upper energy level E_q for the determination of the plasma temperature.

obtained from linear regression of sixteen data points, and the electron temperature was found to be about 9400 K. The average axial temperature for iron samples which were oxidized and for the samples that were doped with sulfur or oxygen was determined to be roughly 8000 K (Table VIII). Again, an estimation of the error in temperature is presented in the Appendix. The electron temperature was utilized to determine the extent of ionization of the plasma during laser welding.

D. *Number Density of Electrons in the Plasma*

A formalism used by Dunn and Eagar[31] was adopted for the calculation of the number density of electrons in the plasma. For a reaction of an atom forming an ion and an electron, *i.e.*, Atom = Ion + Electron, the number densities of ions, electrons, and neutral atoms are given by Saha's equation:[32]

$$\frac{n_e n_i}{n_a} = \frac{Z_e Z_i (2\pi m_e kT)^{3/2} e^{(-V/kT)}}{Z_a h^3} \quad [5]$$

where n_e, n_i, and n_a are particle number densities of electrons, ions, and neutral atoms, respectively, T is the absolute temperature, V is the ionization potential, m_e is the rest mass of an electron, k is the Boltzmann's constant, and h is the Planck's constant. In Eq. [5], the internal partition functions, Z_e, Z_i, and Z_a, are given by

$$Z = \sum_j g_j e^{-u_j/kT} \quad [6]$$

where g_j is the degeneracy or statistical weight corresponding to the energy level u_j. For a monatomic gas,

$$g = 2S + 1 \quad [7]$$

where S is the vector sum of the spin numbers. The partition functions were calculated from the data given in the NBS tables of atomic energy levels compiled by Moore.[33] The degeneracy of electrons was taken as equal to two. The number densities of the ions, electrons, and atoms were obtained by solving Eq. [5] along with Eqs. [8] and [9], which represent the equations of quasi-neutrality of charge and the ideal gas behavior, respectively. Furthermore, kinetic equilibrium ($T_e = T_i = T_a = T$) was assumed for the calculation scheme.

$$n_e = n_i \quad [8]$$

$$n_e + n_i + n_a = 7.34 \times 10^{27}/T \quad [9]$$

The number densities of ions or electrons of each of the pure species, *viz.*, Fe, Cr, Mn, and He, present in the plasma were calculated at various temperatures. These values are plotted in Figure 10. The total electron density, n_e, was determined by multiplying the individual electron densities of pure species by the mole fraction of the representative species and adding the contributions from each species. Complete mixing of the shielding gas with the vaporized material was assumed to determine the composition of the various species in the domain of calculation. The calculated values of the mole fractions of the various species used for the computations are presented in Table V. A plot of the number density of electrons in the plasma as a function of the electron temperature is presented in Figure 10. From the average

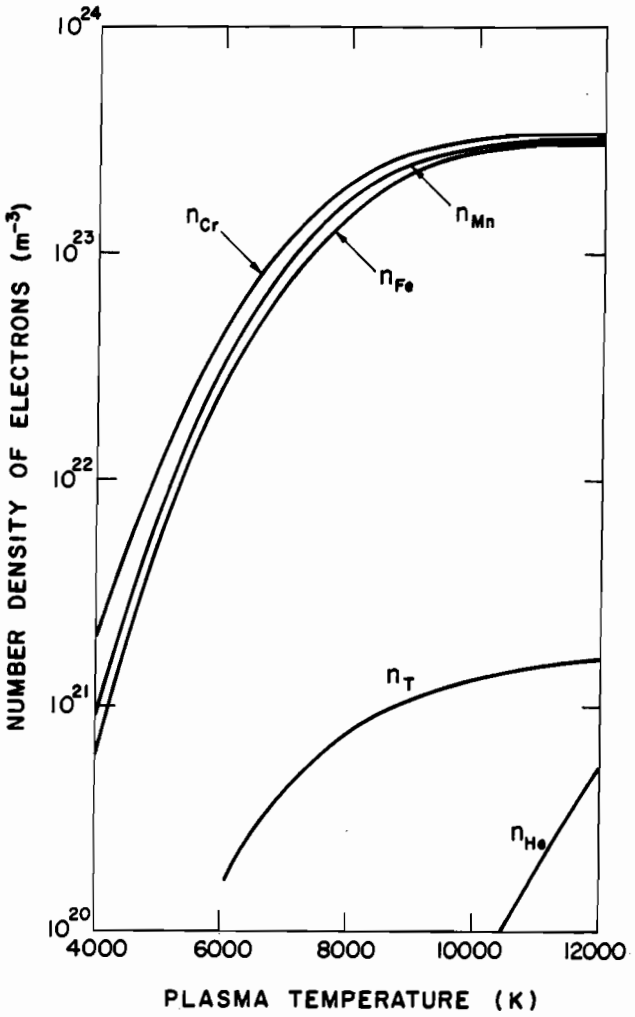

Fig. 10—A plot of the number density of electrons as a function of the electron temperature for Cr, Mn, Fe, and He plasmas and for the plasma present during laser welding of stainless steels.

plasma temperature of about 7000 K for AISI 201 stainless steel, the total electron density in the plasma is determined to be about $4.4 \times 10^{20}/m^3$. The proportion of ionized species at 7000 K, expressed as a percentage of the total number density of all species, was found to be about 0.042 pct (Table VI). The low value of ionization is consistent with the dominance of excited neutral atoms in the plasma (Figure 3). This indicates that the plasma is fairly weak, and the assumption of an optically thin plasma is justified.

Table V. Plasma Composition Used for the Calculation of Number Density

Vaporization Rate = 0.35×10^{-6} kg/s
Helium Gas Flowrate = 3.33×10^{-5} m³/s
J_{Fe}/J_{Mn} (Molar Ratio) = 1.16
J_{Cr}/J_{Mn} (Molar Ratio) = 0.30

Element	Mole Pct
Fe	0.2011
Mn	0.1733
Cr	0.0512
He	99.5740

Table VI. Calculated Number Densities of Ions, Electrons, and Atoms Present in the Plasma at 7000 K

Number Density of Electrons or Ions (m^{-3}) ($n_e - n_i$)	Number Density of Atoms (m^{-3}) n_a	n_i/n_a
0.4407×10^{21}	0.1048×10^{25}	4.205×10^{-4}

E. *Role of Sulfur and Oxygen*

Data in Table VII indicate that the apparent (time average) rate of vaporization of iron from samples doped with sulfur was higher than that from the pure iron samples. Since sulfur is a surface active element, its presence leads to a depletion of free electrons at the surface, resulting in an increase in the absorption of the laser beam.[23] The increase in the apparent vaporization rate due to the presence of sulfur is consistent with the enhanced absorption of the laser beam and the local surface agitation due to interfacial turbulence phenomena.[37] Minor amounts of surface active elements such as sulfur and oxygen present in the base metal can have a significant effect on the vaporization rate and the chemical composition of the weldment. In extreme cases, this can lead to the lack of reproducibility in the composition of the weldments of base materials containing various amounts of surface active impurities.

Figure 11 depicts the spectrum obtained from the plasma produced during laser welding of an iron sample doped with sulfur (0.013 wt pct). On comparing this spectrum with that obtained from the plasma produced from an ultrapure iron sample under similar conditions of welding (Figures 8 and 11), it is observed that the addition of sulfur increases the intensities of the iron peaks. The increase in the intensity of the iron peaks resulting from the presence of sulfur in the alloy was also observed by Savitskii and Leskov[6] and Dunn *et al.*[12] for the arc welding of commercial alloys. Similar increases in the intensities of the iron peaks and the apparent vaporization rates (Table VII) were observed for the oxygen-doped and the oxidized samples as compared to pure iron samples. The increased apparent vaporization rate from the doped and the oxidized samples results in an increase in the number density of atoms in the ground state (n_o).

Table VII. Comparison of the Apparent Rate of Vaporization of Iron from Ultrapure Iron Samples

Sample	Vaporization Rate (mgs/s)
Fe	0.124
Fe-S[a]	0.360
Fe-O[b]	0.216
FeO[c]	0.550*

*Rate of weight loss.
[a]Sulfur doped iron sample (Fe-S).
[b]Oxygen doped iron sample (Fe-O).
[c]Oxidized iron sample (FeO).
Helium flow rate: 3.33×10^{-5} m^3/s; welding speed: 0.005 m/s; current: 35 mA; pulse length: 0.003 s; frequency: 100 Hz.

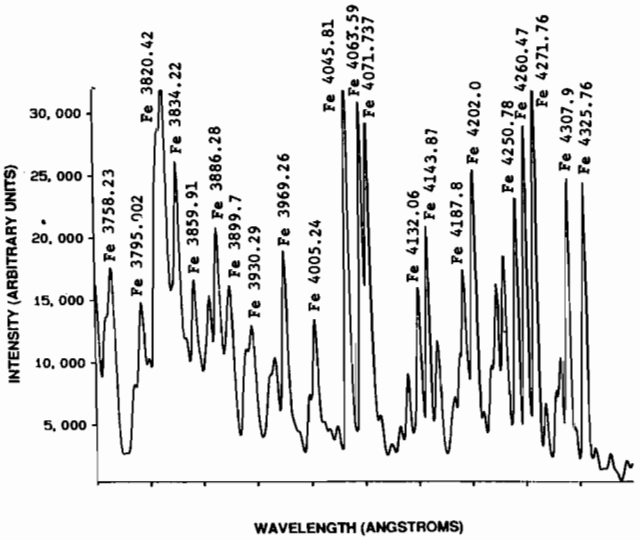

Fig. 11—A typical spectrum of the plasma produced during laser welding of ultrapure iron samples doped with sulfur using helium as the shielding atmosphere. (Gas flow rate = 3.33×10^{-5} m^3/s; welding speed = 0.005 m/s; current = 35 mA; pulse length = 0.003 s; frequency = 100 Hz.)

The number density of atoms at the upper excited energy level (n_{aq}) in the plasma also increases according to Boltzmann distribution (Eq. [2]). This, in turn, contributed to the higher intensity of emission (Eq. [1]) observed in the spectra obtained from Fe-S, Fe-O, and oxidized iron samples. It should be noted that the increased intensity is not significantly contributed by changes in the electron temperatures in the plasma for the various samples, as can be noted from the values presented in Table VIII.

IV. SUMMARY AND CONCLUSIONS

High manganese stainless steel (AISI 201) samples were welded with a carbon dioxide laser at a peak power density of 1.2×10^6 watts/cm^2. The dominant species in the plasma were found to be iron, manganese, and chromium, which were present primarily in their excited neutral states. When the welding was conducted at constant

Table VIII. Electron Temperatures during Laser Welding of Various Samples

System	Temperature (K)
Fe	9406^{+3870}_{-2159}
Fe-S	7995^{+2826}_{-1655}
Fe-O	8040^{+2882}_{-1678}
FeO	7995^{+2844}_{-1661}

Note: The errors reported are with 80 pct confidence limits. Helium flow rate: 3.33×10^{-5} m^3/s; welding speed: 0.005 m/s; current: 35 mA; pulse length: 0.003 s; frequency: 100 Hz.

welding speed, shielding gas flow rate, and composition, an increase in the vaporization rate was found to be accompanied by a concomitant increase in the intensities of various peaks. The electron temperature was found to be between 6500 and 9400 K. The extent of ionization of various species in the plasma under the conditions of welding is demonstrated to be very small. When experiments were performed with ultrapure iron samples that were either doped with oxygen or sulfur or were oxidized, the intensities of iron peaks and the vaporization rates were higher in all cases than the corresponding values for the untreated ultrapure iron samples.

APPENDIX

Estimation of errors in electron temperatures

The radial distribution of temperature shown in Figure 7 was determined from the local emissivities of the two thermometric peaks of manganese using Eq. [3]. The primary source of error in the estimation of temperature is the uncertainty in the transition probability data. Since these errors in the available data cannot be estimated with a predetermined level of confidence, the uncertainties in the temperatures presented in Figure 7 cannot be estimated with a sufficient level of confidence; and, therefore, the errors are not indicated in this figure. However, a rough estimation of the error in temperature was made assuming an error of ±25 pct in the transition probability data. The upper limit of the temperature was determined by decreasing the transition probability of Mn 5377.63 Å line by a factor of 25 pct, increasing the transition probability of Mn 5341.06 Å line by a factor of 25 pct, and calculating a new temperature value using Eq. [3]. The lower limit of the temperature was determined in a similar manner by appropriately changing the values of the two transition probabilities for the two peaks by 25 pct. The average errors in the ten values of electron temperatures reported in Figure 7 are +22 pct and −15 pct for the upper and lower limits, respectively.

The errors in the electron temperatures reported in Table VIII were calculated from the uncertainties in the slopes of the plots used to determine temperature values such as the one presented in Figure 9. The errors correspond to an 80 pct confidence interval for the slope and were calculated by a standard regression technique.[38] It is to be noted that the slope of the plot in Figure 9 is a nonlinear function of electron temperature. Although statistically the slope has equal uncertainties in both upper and lower limits, this does not translate into equal errors in the upper and lower limits of temperature values because of the hyperbolic relation between the slope of the line and the temperature.

DEDICATION

It was a privilege to present a paper at the Symposium on Physical Chemistry in Metals Processing dedicated to the memory of an outstanding educator and scientist, Dr. T.B. King.

ACKNOWLEDGMENT

This work was sponsored by the United States Department of Energy, Office of Basic Energy Sciences, Division of Materials Science, under Grant No. DE-FG02-84ER45158.

REFERENCES

1. L.R. Hettche, E.A. Metzbower, J.D. Ayers, and P.G. Moore: *Naval Research Reviews*, 1981, vol. 28, pp. 4-20.
2. P.A.A. Khan and T. DebRoy: *Metall. Trans. B*, 1984, vol. 15B, pp. 641-44.
3. M.M. Collur, A. Paul, and T. DebRoy: *Metall. Trans. B*, 1987, vol. 18B, pp. 733-40.
4. P. Sahoo and T. DebRoy: *Metall. Trans. B*, 1987, vol. 18B, pp. 597-601.
5. E.V. Locke, E.D. Hoag, and R.A. Hella: *Welding J.*, 1972, vol. 51, pp. 245s-49s.
6. M.M. Savitskii and G.I. Leskov: *Automatic Welding*, 1980, vol. 33 (9), pp. 11-16.
7. S.S. Glickstein: *Welding J.*, 1976, vol. 55, pp. 222s-29s.
8. C.B. Shaw, Jr.: *Welding J.*, 1975, vol. 54, pp. 33s-44s.
9. W.S. Bennett and G.S. Mills: *Welding J.*, 1974, vol. 53, pp. 548s-53s.
10. J.C. Metcalfe and M.B.C. Quigley: *Welding J.*, 1977, vol. 56, pp. 133s-39s.
11. J.F. Key, M.E. McIlwain, and L. Isaacson: in *6th Int. Conf. on Gas Discharges and Their Applications*, Conf. Publ. No. 189, part 2, Institution of Electrical Engineers, New York, NY, 1980, pp. 235-38.
12. G.J. Dunn, C.D. Allemand, and T.W. Eagar: *Metall. Trans. A*, 1986, vol. 17A, pp. 1851-63.
13. G.S. Mills: *Welding J.*, 1977, vol. 56, pp. 186s-88s.
14. G.S. Mills: *Welding J.*, 1977, vol. 56, pp. 93s-96s.
15. J.C. Chennat and C.E. Albright: *Proc. of the Int. Cong. of Application of Lasers and Electron Optics (ICALEO)*, Laser Institute of America, 1984, vol. 44, pp. 76-85.
16. T.J. Rockstroh and J. Mazumder: *J. of Applied Physics*, 1987, vol. 61 (3), pp. 917-23.
17. J.T. Knudtson, W.B. Green, and D.G. Sutton: *J. of Applied Physics*, 1987, vol. 61 (10), pp. 4771-80.
18. Y. Arata, S. Miyake, H. Matsuoka, and H. Kishimoto: *Trans. JWRI*, 1981, vol. 10, pp. 33-38.
19. E.T. Turkdogan, S. Ignatowicz, and J. Pearson: *J. of the Iron and Steel Inst.*, 1955, vol. 180, pp. 349-54.
20. J.A. Kitchener, J.O'M. Bockris, M. Gleiser, and J.W. Evans: *Acta Metall.*, 1953, vol. 1, pp. 93-101.
21. P.W.J.M. Boumans: *Theory of Spectrochemical Excitation*, Hilger and Watts Ltd., London, 1966.
22. *Handbook of Chemistry and Physics*, 64th ed., R.C. Weast, ed., 1983–84, CRC Press, Inc., pp. E–192-E–318.
23. P.A.A. Khan: Ph.D. Thesis, The Pennsylvania State University, University Park, PA, 1987.
24. W.L. Barr: *J. of the Optical Society of America*, 1962, vol. 52, pp. 885-88.
25. J.R. Fuhr: Data Center on Atomic Transition Probabilities, Center for Radiation Research, National Bureau of Standards, private communication, Aug. 1987.
26. A.N. Pirri, N.H. Kemp, R.G. Root, and R.K.S. Wu: *Theoretical Laser Effects Studies*, Final Report No. PSI-TR-89, Physical Sciences Inc., Jan. 1977.
27. T.J. Rockstroh: Ph.D. Thesis, University of Illinois at Urbana-Champaign, 1987.
28. G. Bekefi: *Principles of Laser Plasmas*, Wiley, New York, NY, 1976.
29. H.R. Griem: *Plasma Spectroscopy*, McGraw-Hill, New York, NY, 1964.
30. J.T. Fuhr, G.A. Martin, W.L. Wiese, and S.M. Younger: *J. Phys. Chem. Reference Data*, 1981, vol. 10 (2), pp. 327-87.
31. G.J. Dunn and T.W. Eagar: *Metall. Trans. A*, 1986, vol. 17A, pp. 1865-71.
32. C. Weisman: *Welding Handbook*, 7th ed., AWS, Miami, FL, 1976, vol. 1, p. 52.

33. C.E. Moore: *Atomic Energy Levels*, NSRDS-NBS 35, NBS, Washington, DC, 1971, vols. 1–3.
34. G.V. Marr: *Plasma Spectroscopy*, Elsevier Publishing Company, Ltd., New York, NY, 1968, pp. 278-79.
35. H.N. Olsen: *The Physics of Fluids*, 1959, vol. 2, pp. 614-23.
36. H.C. Peebles and R.L. Williamson: *Proc. of Int. Conf. on Laser Advanced Materials Processing*, Osaka, Japan, May 21–23, 1987, pp. 19-24.
37. F.D. Richardson: *Physical Chemistry of Melts in Metallurgy*, Academic Press, London, 1974, vol. 2, pp. 452-53.
38. L. Ott: *An Introduction to Statistical Methods and Data Analysis*, 2nd ed., PWS Publishers, Boston, MA, 1984, pp. 284-85.